Powder Technology 433 (2024) 119299

Contents lists available at ScienceDirect

Powder Technology

journal homepage: www.journals.elsevier.com/powder-technology

Influence of crystal structure on the thermophysical properties and figures-of-merit of propylene glycol: water-based SiC nanofluids

Javier P. Vallejo [a,*], Lara Febrero-Garrido [a], Antón Cacabelos [a], Arturo González-Gil [a], Luis Lugo [b]

[a] *Centro Universitario de la Defensa en la Escuela Naval Militar, Grupo InTeam, Plaza de España, s/n, 36920 Marín, Spain*
[b] *Universidade de Vigo, Grupo GAME, Departamento de Física Aplicada, 36310 Vigo, Spain*

HIGHLIGHTS

- SiC crystal structure does not affect the density and heat capacity of nanofluids.
- β-SiC nanofluids, ↑12%, show higher thermal conductivity than α-SiC nanofluids, ↑4%.
- α-SiC nanofluids, ↑7%, present lower dynamic viscosity than β-SiC nanofluids, ↑17%.
- Monf/Mobf ratios of α-SiC and β-SiC nanofluids are ≥1 in laminar and turbulent flow.
- The least complex crystal structure (β-SiC, cubic) entails superior heat transfer.

GRAPHICAL ABSTRACT

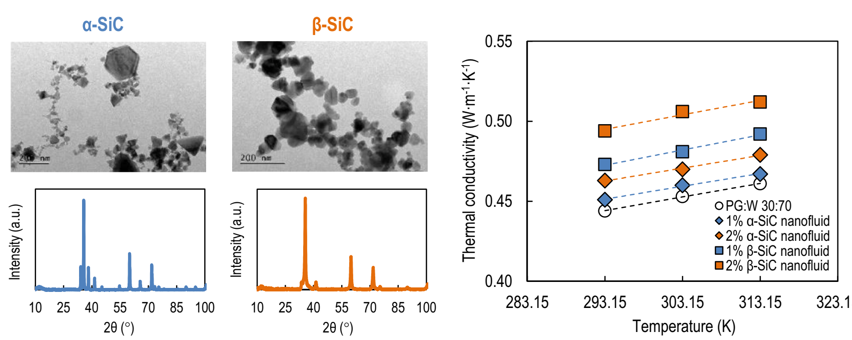

ARTICLE INFO

Keywords:
Nanofluids
Thermophysical properties
Figure-of-merit
Silicon carbide
Crystal structure
Propylene glycol

ABSTRACT

Silicon carbide is a material with a promising thermal conductivity. However, no literature has been found on SiC nanofluids based on propylene glycol:water mixtures (widely used in renewable installations). Likewise, the contribution of α-SiC and β-SiC to the thermophysical properties of nanofluids has scarcely been explored. In this work, dispersions of α-SiC and β-SiC on propylene glycol:water 30:70 wt% at 1 and 2% wt% concentration are designed. Densities, thermal conductivities, dynamic viscosities, and isobaric heat capacities from 293.15 to 313.15 K are obtained by vibrating tube densimetry, transient-hot-wire technique, rotational rheometry and differential scanning calorimetry, respectively. Convective heat transfer performance is also assessed using figures-of-merit. Thermal conductivity and viscosity show a greater dependence on the crystal structure. The β-SiC nanofluids present the highest increases of thermal conductivity (12%) and dynamic viscosity (17%). The least complex crystal structure (β-SiC) exhibits better prospects for convection applications both for laminar and turbulent flow.

1. Introduction

Energy is essential for humanity's survival and progress. The incessant demand for energy due to continuous population growth and industrial development is a challenge for global economic development, making the long-term sustainability of energy supply systems

* Corresponding author.
E-mail address: jvallejo@cud.uvigo.es (J.P. Vallejo).

https://doi.org/10.1016/j.powtec.2023.119299
Received 18 October 2023; Received in revised form 6 December 2023; Accepted 16 December 2023
Available online 18 December 2023
0032-5910/

indispensable. In addition, the emission of gases caused by the consumption of fossil fuels to produce energy is considered the main cause of global warming and climate change. Building energy consumption is responsible for around 40% of total energy demand and 36% of greenhouse gas emissions in Europe [1,2]. Therefore, energy saving and merging renewable resources in existing energy systems is currently one of the most relevant concerns of the scientific community. Technologies such as solar photovoltaic, solar thermal, and geothermal heat pump systems are the most common forms of renewable energy [3]. About 70% of energy consumption is used in heating and cooling [4,5]. Thus, it is essential to limit the rise of energy consumption by enhancing the heat transfer efficiency of real systems. Therefore, it is essential to limit the energy consumption of the systems by improving heat transfer efficiency.

Heat exchangers are the devices through which heat transfer is articulated. Improvements in active and passive methods have provided greater efficiency to heat exchangers. Among the passive methods, surface modifications of heat exchangers have been the most developed techniques historically [6], while the use of nanofluids has begun to stand out in recent years. Nanofluids are dispersions of solid additives of nanometric size within the base fluid that may improve thermal conductivity (which influences greatly in heat transfer), as well as the modification of other physical properties. For the implementation of these improved working fluids, it is necessary to study their synthesis, stability, and thermophysical properties [7]. It is of special relevance the precise and rigorous determination of their thermophysical properties: density (ρ), thermal conductivity (k), dynamic viscosity (η), and isobaric heat capacity (c_p) [8–10]. The most used base fluids in the design of nanofluids are water, glycols and oils. On the other hand, the most frequent nanoparticles in the literature are metals, metal oxides and carbon derivatives [6–10]. However, there are also still common limitations such as low increases in thermal conductivity, high increases in viscosity or a lack of dispersion stability over time. For this reason, the search for new nanomaterials continues to be interesting.

In solid materials, thermal energy is transferred through electrons and lattice vibrations. Thermal transport is dominated by free electrons in metals and by lattice vibrations in semiconductors and insulators. The quantisation of the collective lattice vibration energy is called a phonon. In crystalline solids, phonon modes with similar frequency can move throughout the crystal due to atomic periodicity before being scattered by impurities, boundaries, or other phonons. According to the phonon gas model, thermal conductivity is a function of individual mode specific heat capacities, phonon group velocities and phonon mean free path. Amorphous materials do not present long-distance periodicity, so the extended phonon waves are not well defined, nor is the phonon group velocity or phonon mean free path. Based on the atomic disorder, amorphous materials usually have lower thermal conductivity than crystalline materials [11,12]. On the other hand, it is classically assumed for crystalline materials that the increase in the complexity of the crystal structure implies lower thermal conductivities [13,14].

Silicon carbide (SiC) is a semiconductor material with high hardness and strength, elevated thermal conductivity, high melting point, chemical and thermal stability, and oxidation resistance. Such interesting properties make it attractive for multiple applications, especially for high temperatures or harsh environments [15,16]. The three basic crystallographic categories of SiC are cubic (C), hexagonal (H) and rhombohedral (R), and >250 polytypes are recognised. The hexagonal (nH-SiC) and rhombohedral (nR-SiC) polytypes are commonly known as the α-SiC phase, while the cubic (3C-SiC) polytype is commonly known as the β-SiC phase [15,17]. The most common polymorph is α-SiC with a hexagonal crystal structure, which is stable up to 1700 °C. The α-SiC polytypes that are available in bulk form and have more industrial applications are 6H-SiC and 4H-SiC, whose band gaps are 3.03 and 3.26 eV, respectively [15,18]. The β-SiC polymorph has the smallest band gap, 2.26 eV, and is not currently available in bulk form, but arouses a growing interest due to its higher surface area compared to α-SiC [15].

As Table 1 shows, some authors have previously designed SiC nanofluids and studied some of their thermophysical properties. Singh et al. [19] and Yu et al. [20] reported thermal conductivity improvements over 20% and high viscosity increases for 3.7–7.4 vol% dispersions in water (W) of SiC nanoparticles of 170 nm (no info about phase). Li et al. [21,22] showed thermal conductivity enhancements of 16.2% and viscosity increases of up to 65% for 0.2–1 vol% dispersions of SiC nanoparticles of 30 nm (no info about crystal structure) in ethylene glycol (EG) by using a surfactant. The improvements in thermal conductivity rise to 53.8% and the dynamic viscosity increases are reduced to 22–23% changing the base fluid by ethylene glycol:water at 40:60 vol % (EG:W 40:60 vol%) [23,24]. On the other hand, the increases reach 7.4% and 220%, respectively, if the base fluid is a diathermic oil [25]. Timofeeva et al. [26,27] presented thermal conductivity improvements of 12.5% and 16.5% and viscosity increases of up to 80% and 65% for 4 vol% dispersions of α-SiC (between 16 and 90 nm) in ethylene glycol: water 50:50 vol% (EG:W 50:50 vol%), respectively. Hosseini et al. [28] and Al-Waeli et al. [29] reported thermal conductivity improvements of 15.5% and 8.2% for 1 to 4–5 wt% dispersions of β-SiC nanoparticles (between 20 and 65 nm) in pure ethylene glycol and water, respectively. Huminic et al. [30] and Akilu et al. [31] noticed thermal conductivity improvements of 17.6, 14.6 and 4.8% and viscosity increases of ~30, 78.7, and 55.9% for 0.5–3 wt% dispersions of β-SiC nanoparticles (between 25 and 29 nm) in water, pure ethylene glycol and pure propylene glycol, respectively.

As observed, the most widely used base fluids in SiC nanofluids are water, ethylene glycol, and their binary mixtures. The propylene glycol: water mixture at a mass ratio of 30:70 (PG:W 30:70) offers protection against freezing down to −12.8 °C [3]. It is a working fluid widely used in geothermal and solar thermal installations due to the low temperatures to which they can be exposed in cold outdoor environments. No studies on SiC nanofluids based on mixtures of propylene glycol: water have been found. Table 1 also shows that phase or crystal structure information of SiC nanofluids is not always provided and only one work compares the contribution of α-SiC and β-SiC to the thermal conductivity and dynamic viscosity of nanofluids [36]. Besides, the most extensively analysed thermophysical properties are thermal conductivity and viscosity, but very few works report experimental data on density and heat capacity. Furthermore, there is no literature that estimates the heat transfer performance in convection applications for α-SiC and β-SiC nanofluids.

In this work, new nanofluids based on the PG:W 30:70 mixture are designed, consisting of dispersions of α-SiC and β-SiC with nanoparticle sizes between 25 and 50 nm at 1 and 2 wt% concentrations. Vibrating tube densimetry, transient-hot-wire, rotational rheometry, and differential scanning calorimetry techniques were used to experimentally determine their density, thermal conductivity, dynamic viscosity, and isobaric heat capacity, respectively. The results are compared based on the crystal structure of the SiC nanoparticles and the effectiveness of various theoretical or semiempirical models is verified. Finally, various figures-of-merit and ratios between these thermophysical properties are evaluated to assess the potential performance of heat transfer and pumping power in tubular heat exchangers.

2. Materials and methods

2.1. Materials

Propylene glycol was provided by Merck (Darmstadt, Germany) and Milli-Q deionised water was obtained using a Stakpure OmniaTap (Niederahr, Germany). Mainly hexagonal phase silicon carbide nanopowder (hereinafter α-SiC) and cubic phase silicon carbide nanopowder (hereinafter β-SiC) were provided by PlasmaChem (Berlin, Germany). Table 2 shows the commercial names and the main characteristics of the nanopowders according to the supplier. The nanofluids were prepared with the two-step method at two mass concentrations of nanoadditives:

Table 1
Summary of the available literature on experimental thermophysical properties of SiC nanofluids.

Reference	Nanoadditive	Base fluid	Particle size range	Concentration range	Temperature range	Maximum k increase	Maximum η increase	Maximum ρ increase	Maximum c_p increase
Xie et al. [32]	SiC (spherical, cylindrical)	W, EG	26 nm (spherical), 600 nm (cylindrical)	0.8–4.2 vol%	4 °C	15.8% (spherical, W), 22.9% (cylindrical, W),	–	–	–
Singh et al. [19]	SiC	W	170 nm	4–7.4 vol%	21–70 °C (k), 15–55 °C (η)	28%	~170%	–	–
Yu et al. [20]	SiC	W	170 nm	3.7 vol%	25–70 °C	22%	80–100%	–	–
Hosseini et al. [28]	β-SiC	EG	20–30 nm	1–5 wt%	25 °C	15.55%	–	–	–
Timofeeva et al. [26]	α-SiC	W	16–90 nm	4.1 vol%	22,5 °C (k), 15–35 °C (η)	~12.5%	~80%	–	–
Timofeeva et al. [27]	α-SiC	EG:W 50:50 vol %	16–90 nm	4 vol%	22.5 °C (k), 15–85 °C (η)	~16.5%	~65%	–	–
Lee et al. [33]	SiC	W	<100 nm	0.001–3 vol%	22–23.5 °C (k), 28–72 °C (η)	7.2%	102%	–	–
Manna et al. [34]	SiC	W	27 nm	0.01–0.1 vol%	–	12%	–	–	–
Nikkam et al. [35]	α-SiC	W, EG:W 50:50 wt%	115 nm	3–9 wt%	20 °C	15.2% (W), 20% (EG:W 50:50 wt%)	22.7% (W), 14% (EG:W 50:50 wt%)	–	–
Nikkam et al. [36]	α-SiC, β-SiC	EG:W 50:50 wt %	30–60 nm (α-SiC), 85–115 nm (β-SiC)	9 wt%	20 °C	20% (α-SiC), 14% (β-SiC)	14% (α-SiC), 36% (β-SiC)	–	–
Li et al. [21]	SiC	EG (+PVP, NaOH)	30 nm	0.2–1 vol%	20–50 °C	16.21%	–	–	–
Li et al. [22]	SiC	EG (+dispersant)	30 nm	0.2–1 vol%	25–60 °C	–	~65%	–	–
Akilu et al. [37]	SiC	Glycerol:EG 60:40 wt%	29 nm	0.3–1 vol%	30–60 °C	12.1%	~130%	–	–
Li and Zou [23]	SiC	EG:W 40:60 vol % (+PVP)	30 nm	0.2–1 vol%	10–50 °C	53.81%	~22–23%	~2.1%	–
Li et al. [24]	SiC	EG:W 40:60 vol %	30 nm	0.1–0.5 vol%.	10–50 °C	53.81%	~22–23%	–	–
Li et al. [25]	SiC	Diathermic oil	30 nm	0.2–0.8 vol%	20–50 °C (k), 25–60 °C (η)	7.36%	~220%	–	–
Yu et al. [38]	β-SiC (nanowires)	EG	0.2–1 μm diameter, 3–40 μm length	1–5 vol%	20–70 °C	67.2%	–	–	–
Al-Waeli et al. [29]	β-SiC	W	45–65 nm	1–4 wt%	25–60 °C	8.2%	1.8%	0.0082%	–
Chen et al. [39]	SiC	W (Saline)	30 nm	0.4 vol%	10–50 °C	5.2%	–	–	–
Chen et al. [40]	SiC	$[HMIM]BF_4$ ionic liquid	30 nm	0.01–0.06 wt%	25–65 °C (k, η, ρ), 0–80 °C (c_p)	~10%	~15%	~5%	5%
Huminic et al. [30]	β-SiC	W	25 nm	0.5–1 wt%	20–50 °C	17.62%	~30–40%	–	–
Akilu et al. [31]	β-SiC	EG, PG	29 nm	0.72–3 wt%	298.15–353.15 K	14.6% (EG), 4.8% (PG)	78.7% (EG), 55.9% (PG)	–	–
Ezekwem and Dare [41]	α-SiC	W, EG	23.85 nm	0.5–5 vol%	28 °C	16% (W), 25% (EG)	–	–	–
Ajeeb and Murshed [41]	SiC	EG:W 30:70 vol %	50–60 nm	0.01–0.05 vol %	20 °C (k, ρ), 22–41 °C (η)	4.4%	5.2%	0.3%	–

1 and 2%. For this, the corresponding amounts of the constituents of the base fluid and of the nanoadditives were weighed on a Gram FV-220C analytical balance (Barcelona, Spain) with a precision of $1 \cdot 10^{-4}$ g. The mixtures were then sonicated in an Elmasonic S 300H bath from Elma (Singen, Germany) for 180 min at 300 W and 37 kHz. For a SiC density value of 3210 $kg \cdot m^{-3}$ (both for α and β phase) [42,43], the 0.01 and 0.02 mass fractions correspond to 0.00321 and 0.00647 volume fractions, respectively.

2.2. Methods

2.2.1. Experimental methods

The morphological characteristics of the nanoparticles were examined by transmission electron microscopy (TEM) using a JEM-1010 microscope from JEOL (Tokyo, Japan) at 100 kV. The images were captured on a carbon-coated copper grid on which a drop of each nanopowder dispersion in analytical grade ethanol was deposited and allowed to dry. The crystal structure of the nanoparticles was examined by X-ray diffraction (XRD) analyses of the nanopowders using a D-5000 diffractometer from Siemens (Karlsruhe, Germany) with CuKα radiation

Table 2
Main characteristics of the silicon carbide nanopowders according to the supplier.

Nomenclature	α-SiC	β-SiC
Commercial name	Silicon carbide nanopowder, grade PJ	Silicon carbide nanopowder, grade HK
Provider	PlasmaChem	PlasmaChem
Appearance	Gray powder	Gray powder
Average particle size (nm)	25–50	25
Specific surface area ($m^2 \cdot g^{-1}$)	18	80
Density ($g \cdot cm^{-3}$)	0.23–0.35	0.15–0.25
Phase	98% hexagonal	cubic
Purity	> 98.6%	> 99.0%
pH, 10 $mg \cdot mL^{-1}$ aqueous	7,1	7,1
Controlled admixtures	Cu < 0.4%, W < 0.2%, Fe < 0.1%, Al < 0.03%, Mg < 0.03%, Na < 0.03%	C (free) < 1%, Si (free) < 0.75%, O < 1.25%, Cl < 0.25%

in the 2θ range from 10 to 100°. The zeta potential of the nanofluids was determined at 293.15 K by a Zetasizer Nano ZS device from Malvern Instruments (Malvern, UK). The tests were conducted in DTS1070 cells.

The density (ρ) of the base fluid and the nanofluids was determined using the oscillating U-tube technique at 293.15, 303.15 and 313.15 K. A DMA 4100 M densimeter from Anton Paar (Graz, Austria) was used. The sample temperature was stabilised by Peltier control. The expanded uncertainty (k = 2) of obtained density values was previously stated as 0.1% [44].

The thermal conductivity (k) of the base fluid and the nanofluids was determined by the transient-hot-wire technique at 293.15, 303.15 and 313.15 K. A TEMPOS thermal properties analyser from the METER group (Pullman, Washington, USA) was used, attached with a KS-3 sensor (diameter = 1.3 mm, length = 60 mm). The temperature of the samples was guaranteed by a hermetic air chamber. The KS-3 needle works both as a heat source and as a temperature sensor and allows thermal conductivity measurements in the range from 0.02 to 2 $W \cdot m^{-1} \cdot K^{-1}$. The low power measurement mode was used in which slight heat is applied to the needle, helping to prevent free convection in liquids. The manufacturer states a 5% accuracy in the thermal conductivity range from 0.2 to 2 $W \cdot m^{-1} \cdot K^{-1}$.

The rheological behaviour of the base fluid and the nanofluids was determined at 293.15, 303.15 and 313.15 K by rotational rheometry using a Physica MCR 101 rheometer from Anton Paar (Graz, Austria) with CP50–1 cone-plate geometry (diameter = 50 mm, cone angle = 1°). A Peltier system guaranteed the temperature achievement and maintenance. The tests were carried out in the shear rate range from 10 to 1000 s^{-1} at a fixed gap of 0.102 mm. The measurement time was set by the automatic mode to ensure the steady state of the samples at each shear rate. The dynamic viscosity (η) values of the samples were calculated as the mean value in the 100–1000 s^{-1}decade. The expanded uncertainty (k = 2) of the measurements was previously stated as 3% [45].

The isobaric heat capacity (c_p) of the base fluid and the nanofluids was determined by the differential scanning calorimetry (DSC) at 293.15, 303.15 and 313.15 K. A Q2000 differential scanning calorimeter from TA Instruments (Newcastle, United Kingdom) combined with a RSC90 cooling system was used. The measurements were conducted via the quasi-isothermal temperature modulated DSC method in a nitrogen atmosphere using Tzero Pan + Tzero Hermetic Lid cells. The temperature was modulated sinusoidally around the set value (amplitude = 0.5 K, period = 80 s). The expanded uncertainty (k = 2) of the c_p measurements was previously stated as 3% [46].

2.2.2. Figures-of-merit determination

The thermophysical properties of the working fluid play a fundamental role in the efficiency of convective heat transfer applications. This relationship is not direct and depends largely on the operating conditions. However, the literature includes some figures-of-merit based on thermophysical properties to characterize the convection or pumping power performances of fluids relative to its alternatives for certain heat exchangers and conditions.

The Mouromtseff number, Mo, estimates the heat transfer efficiency of alternative thermal fluids in single-phase forced convection with fully developed flow in a circular pipe as a function of density (ρ), thermal conductivity (k), isobaric heat capacity (c_p), and dynamic viscosity (η):

$$Mo = \frac{\rho^{a} \cdot k^{b} \cdot {c_p}^{c}}{\eta^{d}} \tag{1}$$

where the constants a, b, c, and d should be selected from the heat transfer equations of the appropriate heat transfer mode. The influence of k on Mo is always greater than that of η whatever the conditions, so b > d in all cases [47,48]. The ratio between the Mouromtseff number of a nanofluid (nf) and the corresponding base fluid (bf), Mo_{nf}/Mo_{bf}, is equivalent to the ratio between their convective heat transfer coefficients (h), h_{nf}/h_{bf}, at a constant velocity [49].

- Convective heat transfer in laminar flow

For a fully developed internal laminar flow over a pipe, Simons [50] states that only the thermal conductivity affects the heat transfer coefficient because the Nusselt number is constant for a fixed wall temperature or heat flux. Therefore, Mo can be directly assumed as the thermal conductivity of the fluid and the Mo_{nf}/Mo_{bf} ratio can be stated as follows:

$$\left(\frac{Mo_{nf}}{Mo_{bf}}\right)_{\text{laminar flow}} = \frac{k_{nf}}{k_{bf}} \tag{2}$$

A Mo_{nf}/Mo_{bf} ratio >1 would imply that the nanofluid exhibits superior performance than the base fluid. Many other authors have also applied Eq. 2 to compare nanofluids and base fluids [30,51–55].

Prasher [56] introduced another ratio to evaluate the applicability of nanofluids in internal laminar flow, based on the k and η of the nanofluid and the base fluid:

$$\left(\frac{C_\eta}{C_k}\right)_{\text{laminar flow}} = \frac{(\eta_{nf} - \eta_{bf})/\eta_{bf}}{(k_{nf} - k_{bf})/k_{bf}} \tag{3}$$

A C_η/C_k ratio lower than 4 would mean that the nanofluid can effectively replace the base fluid as a thermal fluid. Several authors have also applied Eq. 3 to compare nanofluids and base fluids [30,52–55].

- Convective heat transfer in turbulent flow.

For a fully developed internal turbulent flow over a pipe, the criterion based on the Mo_{nf}/Mo_{bf} ratio is widely applied. However, the literature includes different values for the exponents a, b, c, and d in Eq. (1) depending on the authors. Some of the most used expressions are described as follows.

The Dittus-Boelter equation is given by $Nu = 0.023 \cdot Re^{0.8} \cdot Pr^{n}$, where Nu, Re and Pr means Nusselt, Reynolds and Prandtl number, respectively, and $n = 0.4$ for heating and $n = 0.3$ for cooling of the fluid with fixed wall temperature or heat flux. Several authors applied the exponents obtained from this equation to the Mo_{nf}/Mo_{bf} ratio for both nanofluid and base fluid in heating [57–60] and cooling [49,51] processes.

$$\left(\frac{Mo_{nf}}{Mo_{bf}}\right)_{\substack{\text{turbulent flow} \\ \text{Dittus-Boelter} \\ \text{heating}}} = \frac{\dfrac{{\rho_{nf}}^{0.8} \cdot {k_{nf}}^{0.6} \cdot {c_{p\,nf}}^{0.4}}{{\eta_{nf}}^{0.4}}}{\dfrac{{\rho_{bf}}^{0.8} \cdot {k_{bf}}^{0.6} \cdot {c_{p\,bf}}^{0.4}}{{\eta_{bf}}^{0.4}}} \tag{4}$$

$$\left(\frac{Mo_{nf}}{Mo_{bf}}\right)_{\substack{\text{turbulent flow}\\ \text{Dittus-Boelter}\\ \text{cooling}}} = \frac{\dfrac{\rho_{nf}^{0.8}\cdot k_{nf}^{0.7}\cdot c_{p\ nf}^{0.3}}{\eta_{nf}^{0.5}}}{\dfrac{\rho_{bf}^{0.8}\cdot k_{bf}^{0.7}\cdot c_{p\ bf}^{0.3}}{\eta_{bf}^{0.5}}} \tag{5}$$

Simons [50] also proposed his own values for the exponents for various refrigerants, and several authors used these values to the Mo_{nf}/Mo_{bf} ratio for both nanofluid and base fluid [52,61–64].

$$\left(\frac{\mathrm{Mo_{nf}}}{\mathrm{Mo_{bf}}}\right)_{\substack{\text{turbulent flow}\\ \text{Simons}}} = \frac{\dfrac{\rho_{nf}^{0.8}\cdot k_{nf}^{0.67}\cdot c_{p\ nf}^{0.33}}{\eta_{nf}^{0.47}}}{\dfrac{\rho_{bf}^{0.8}\cdot k_{bf}^{0.67}\cdot c_{p\ bf}^{0.33}}{\eta_{bf}^{0.47}}} \tag{6}$$

Vajjha and Das [65] proposed different values of the exponents in the Mo_{nf}/Mo_{bf} ratio for the base fluid (based on the Dittus-Boelter equation for heating) and the nanofluids (based on the Pak and Cho equation $Nu = 0.021{\cdot}Re^{0.8}{\cdot}Pr^{0.5}$). Various authors have also applied these same values [45,66–69].

$$\left(\frac{Mo_{nf}}{Mo_{bf}}\right)_{\substack{\text{turbulent flow}\\ \text{Vajjha and Das}}} = \frac{\dfrac{\rho_{nf}^{0.8}\cdot k_{nf}^{0.5}\cdot c_{p\ nf}^{0.5}}{\eta_{nf}^{0.3}}}{\dfrac{\rho_{bf}^{0.8}\cdot k_{bf}^{0.6}\cdot c_{p\ bf}^{0.4}}{\eta_{bf}^{0.4}}} \tag{7}$$

- Pumping power in laminar flow

For fully developed laminar flow at a constant velocity over a tube subjected to a uniform heat flux, Mansour et al. [70] stated the following expression to estimate the pumping power consumption ratio, $\dot{W}_{nf}/\dot{W}_{bf}$, as a function of density and dynamic viscosity:

$$\left(\frac{\dot{W}_{nf}}{\dot{W}_{bf}}\right)_{\text{laminar flow}} = \frac{\eta_{nf}}{\eta_{bf}}\cdot\left[\frac{\rho_{bf}}{\rho_{nf}}\right]^2 \tag{8}$$

A $\dot{W}_{nf}/\dot{W}_{bf}$ ratio above 1 would imply that the nanofluid needs more pumping power to flow than the base fluid.

- Pumping power in turbulent flow

For fully developed turbulent flow in the same previous conditions, Mansour et al. [70] proposed the following expression:

$$\left(\frac{\dot{W}_{nf}}{\dot{W}_{bf}}\right)_{\text{turbulent flow}} = \left[\frac{\eta_{nf}}{\eta_{bf}}\right]^{0.25}\cdot\left[\frac{\rho_{bf}}{\rho_{nf}}\right]^2 \tag{9}$$

Eqs. (2)–(9) were used for the comparison of our designed nanofluids and base fluid at the defined operating conditions.

3. Results

3.1. Nanoparticle characterisation and nanofluid stability

Fig. 1 shows the XRD spectrum of the studied commercial nanopowders. In Fig. 1a (α-SiC nanopowder), the diffraction peaks obtained at 2θ angles of 34.1°, 35.7°, 38.2°, 41.4°, 45.3°, 54.7°, 60.0°, 65.6°, 70.9°, 71.8°, 73.4°, 75.4°, 90.0° and 95.0° can be indexed as planes (101), (102), (103), (104), (105), (107), (110), (109), (201), (202), (203), (204), (208), and (209) of 6H-SiC, respectively (Reference code: 00–029-1128). In Fig. 1b (β-SiC nanopowder), the diffraction peaks obtained at 2θ angles of 35.6°, 41.3°, 59.9°, 71.7°, 75.5°, and 89.8° can be indexed as planes (111), (200), (220), (220), (311), (222), and (400) of 3C-SiC, respectively (Reference code: 00–029-1129). Thus, the identified crystal structure fits the phase reported by the supplier.

Fig. 2 shows TEM images of the silicon carbide nanopowders. Not much aggregation of the nanoparticles is observed after the process of dispersion in ethanol and subsequent drying. In both cases, the nanoparticles mostly present flat edges that form different prismatic shapes. Regarding size, Fig. 2 shows nanoparticles with dimensions like those reported by the manufacturer (see Table 2). However, a greater degree of polymorphism is noted for α-SiC nanopowder.

The stability of nanoparticle dispersions in the base fluids is a key issue in the efficiency and applications of nanofluids. Poor stability, i.e. particle agglomeration and precipitation, can mean changes over time in the thermophysical properties and heat transfer performance of the working fluids. Furthermore, deposits and fouling can cause major problems (heat exchangers, pumps). The zeta potential is conceived as a sign of the stability of nanofluids due to its direct relationship with the magnitude of the electrostatic forces that occur between the dispersed particles. Those repulsive forces should be robust enough to prevail over the attractive forces that cause their agglomeration and sedimentation [71]. Zeta potentials >30 mV in absolute value are considered evidence of acceptable stability in colloidal dispersions in liquids with reduced ionic strength such as water or glycol:water mixtures [45,72]. The 1% α-SiC nanofluid presents a zeta potential of −31.7 mV and the 1% β-SiC nanofluid presents a zeta potential of −28.3 mV. Thus, both dispersions show values which are very close to the threshold of 30 mV, so they can be considered moderately stable.

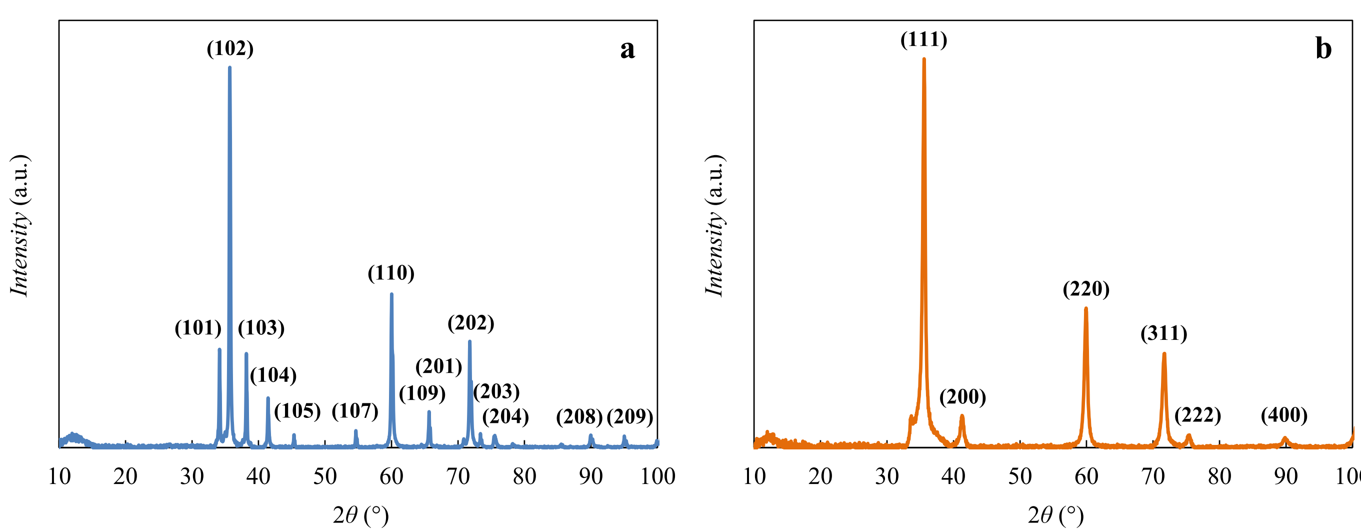

Fig. 1. XRD spectra of α-SiC (a) and β-SiC (b) nanopowders in the 2θ range from 10 to 100°, with the Miller indices of the lattice planes for the main crystal structure identified: 6H-SiC (a) and 3C-SiC (b).

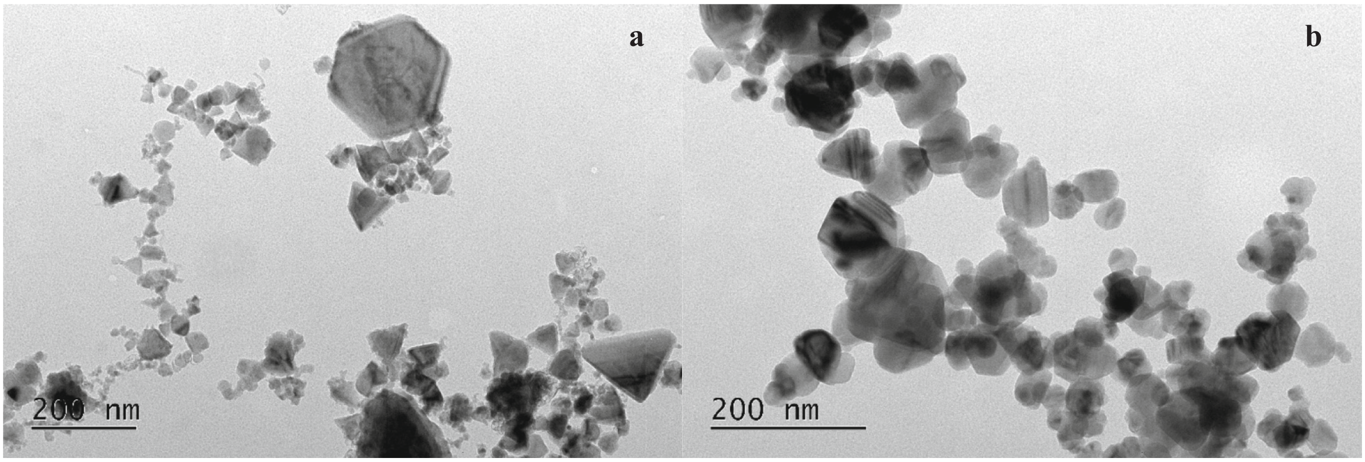

Fig. 2. Transmission electron microscopy images of α-SiC (a) and β-SiC (b) nanopowders at 100 kV acceleration voltage.

3.2. Density

Table 3 shows the obtained density values for PG:W 30:70 and the nanofluids at various temperatures. These experimental values for the base fluid are in good agreement with the literature, with absolute average deviations of 0.050%, 0.077%, 0.049%, 0.020%, and 0.043% with respect to Verline et al. [73], Kapadi et al. [74], Yang et al. [75], Melinder [76] and Vallejo et al. [77], respectively. Fig. 3 shows the identical temperature dependence of density for the base fluid and the nanofluids, since all the samples show a density decrease of around 1% for the temperature increase from 293.15 to 313.15 K.

Regarding the rise in density owing to the addition of nanoparticles, very similar results are found for both α-SiC and β-SiC nanofluids. The 1% nanofluids produce increases in density of 0.6–0.7% with respect to the base fluid, while the 2% nanofluids produce increases of 1.5–1.6%. It can be concluded, therefore, that the crystal structure of silicon carbide does not show a significant influence on the density increase of nanofluids. This result is in accordance with the identical value stated in the literature for the bulk density of 3C-SiC, 6H-SiC, and 4H-SiC at 300 K, 3210 kg·m^{-3} [42,43].

The classical mixing rule for ideal gas mixtures that considers the volume fraction of each constituent has been adapted by Pak and Cho [78] and then extensively validated [79,80] to predict the effective density of nanofluids, assimilating them as elemental solid and liquid mixtures:

$$\rho_{nf} = \phi_v \cdot \rho_{np} + (1 - \phi_v) \cdot \rho_{bf} \tag{10}$$

where ρ is density, ϕ_v is the volume fraction of nanoadditive, and nf, np and bf mean nanofluid, nanoparticle, and base fluid, respectively. Using a ρ_{np} value of 3210 kg·m^{-3}, average deviations of −0.07%, 0.16%, −0.03%, and 0.21% were obtained for the 1% α-SiC, 2% α-SiC, 1% β-SiC, and 2% β-SiC nanofluids, respectively. Therefore, a good agreement between the experimental and predicted data was found. The agreement is slightly better for low nanoparticle concentrations, as observed in Fig. 3, in line with the results reported by other authors [44,80].

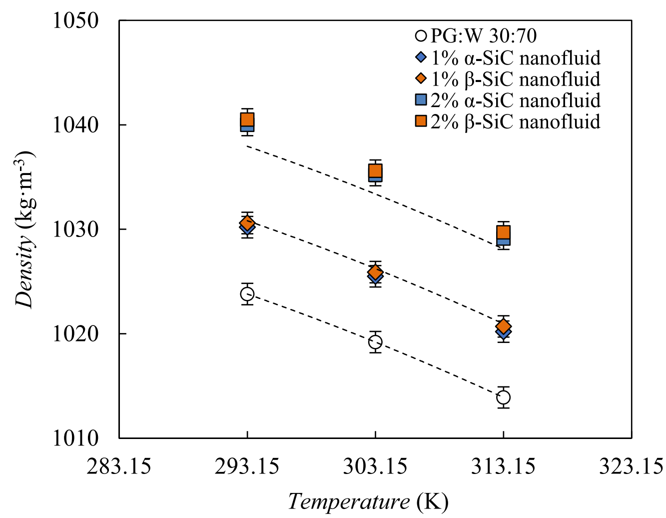

Fig. 3. Density as a function of temperature for PG:W 30:70 base fluid and α-SiC and β-SiC nanofluids at different concentrations. Error bars inform about the expanded uncertainty (k = 2). Reference lines are obtained from Pack and Cho's model with ρ_{np} = 3210 kg·m^{-3}, Eq. 10 (−−).

3.3. Thermal conductivity

Table 4 presents the experimental thermal conductivities for PG:W 30:70 and the nanofluids at the analysed temperatures. The values here reported for the base fluid are in accordance with the literature with absolute average deviations of 2.2% from Bates and Hazzard [81], 0.1%

Table 3
Experimental density values[a] for PG:W 30:70 base fluid and α-SiC and β-SiC nanofluids at different temperatures[b].

Temperature (K)	*Density* (kg·m^{-3})				
	PG:W 30:70	1% α-SiC nanofluid	2% α-SiC nanofluid	1% β-SiC nanofluid	2% β-SiC nanofluid
293.15	1023.8	1030.2	1040.0	1030.6	1040.5
303.15	1019.2	1025.5	1035.2	1025.9	1035.6
313.15	1013.9	1020.2	1029.1	1020.7	1029.7

[a] Expanded uncertainty of density (k = 2): 0.1%.
[b] Expanded uncertainty of temperature (k = 2): 0.1 K.

Table 4
Experimental thermal conductivity values[a] for PG:W 30:70 base fluid and α-SiC and β-SiC nanofluids at different temperatures[b].

Temperature (K)	*Thermal conductivity* (W·m^{-1}·K^{-1})				
	PG:W 30:70	1% α-SiC nanofluid	2% α-SiC nanofluid	1% β-SiC nanofluid	2% β-SiC nanofluid
293.15	0.444	0.451	0.463	0.473	0.494
303.15	0.453	0.460	0.470	0.481	0.506
313.15	0.461	0.467	0.479	0.492	0.512

[a] Expanded uncertainty of thermal conductivity (k = 2): 5%.
[b] Expanded uncertainty of temperature (k = 2): 0.1 K.

from Melinder [76] and 0.3% from Vallejo et al. [77]. Fig. 4 shows the dependence of thermal conductivity with temperature, demonstrating a behaviour between the base fluid and the nanofluids that is not significantly differentiated. Increases of 3.5–4.0% are observed for all samples if temperature rises from 293.15 to 313.15 K.

In relation to the thermal conductivity enhancements because of the dispersion of nanoparticles, it is observed that the crystal structure of the nanopowders plays a noticeable role. The β-SiC nanofluids achieve the greatest increases with respect to the base fluid, reaching 11–12% improvements for the 2 wt% nanoadditive concentration. Conversely, the maximum improvement for the α-SiC nanofluids reaches 4%. Thus, it can be concluded that SiC with a mostly cubic crystal structure provides greater k results than SiC with a mostly hexagonal crystal structure at the same nanoadditive concentration. It should be noted that Nikkam et al. [30] obtained the opposite trend for 9 wt% nanofluids based on EG:W 50:50 wt%. They reported a superior increase for α-SiC nanofluids (around 20%) than for β-SiC nanofluids (around 14%). However, the smaller size of their α-SiC nanoparticles (30–60 nm for Si-α versus 85–115 nm for Si-β), usually linked to a larger specific surface area, could explain this result.

The thermal conductivity of 4H-SiC, 6H-SiC and 3C-SiC polytypes in solid state has been studied in the literature. 4H-SiC presents a k value of around 370 $W \cdot m^{-1} \cdot K^{-1}$ at 300 K [82]. 6H-SiC is frequently associated with a high k of 490 $W \cdot m^{-1} \cdot K^{-1}$, based on thermocouple-based measurements of Slack in 1964 [83]. However, later and more precise measurements have corrected this value [84–89]. As an example, Müller et al. [86], Zheng et al. [88] or Cheng et al. [89] reported k values for 6H-SiC of 340–350 $W \cdot m^{-1} \cdot K^{-1}$ at 300 K. On the other hand, the thermal conductivity of 3C-SiC presents a much greater discrepancy in the literature. Some authors reported lower k values than those of the structurally more complex 6H-SiC polytype [85,86], which contradicts the simple theory prediction that structure complexity and thermal conductivity should be inversely related. Thus, Katre et al. [90] attributed the low k value of 3C-SiC in the literature to the extremely strong boron defect-phonon scattering. Taking this fact into account, Cheng et al. [91] reported a k value >500 $W \cdot m^{-1} \cdot K^{-1}$ for 3C-SiC crystals at room temperature, which is the second greatest among large crystals, surpassed only by diamond. Reinforcing these results, Lim et al. [92] studied the thermal conductivity of ceramics with different ratios between α-SiC and β-SiC powders and concluded that k decreases as α-SiC content increases. Our results for nanofluids suggest that the nanoparticles with the least complex crystal structure (β-SiC, cubic) improve the thermal conductivity of the fluid in which they are dispersed more than those with the most complex crystal structure (α-SiC, hexagonal)—for the same material and maintaining similar morphological characteristics (size, shape, specific surface area)—, in accordance with the theory prediction about structure complexity.

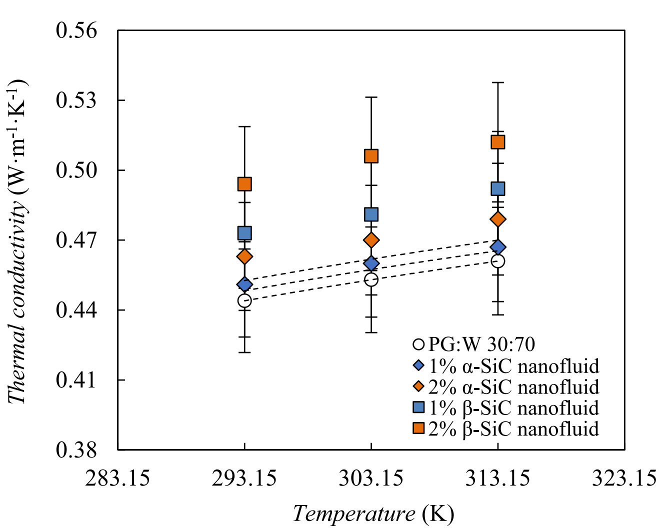

Fig. 4. Thermal conductivity as a function of temperature for PG:W 30:70 base fluid and α-SiC and β-SiC nanofluids at different concentrations. Error bars inform about the expanded uncertainty (k = 2). Reference lines are obtained from Maxwell model with $k_{np} = 350\ W \cdot m^{-1} \cdot K^{-1}$, Eq. 11 (−−).

Many theoretical models have been proposed in the literature for the thermal conductivity prediction of nanofluids. Many of them have been based on classical models of thermal conductivity [93]. One of the first classical models used with nanofluids is Maxwell's model [94], initially conceived for solid-liquid mixtures with small particle fractions of randomly dispersed spheres that do not interact with each other:

$$k_{nf} = \frac{k_{np} + 2 \cdot k_{bf} + 2 \cdot \phi_v \cdot (k_{np} - k_{bf})}{k_{np} + 2 \cdot k_{bf} - \phi_v \cdot (k_{np} - k_{bf})} \cdot k_{bf} \tag{11}$$

where k is thermal conductivity, ϕ_v is the volume fraction of nanoadditive, and nf, np and bf mean nanofluid, nanoparticle, and base fluid, respectively. Hamilton-Crosser [95] further developed Maxwell's model, considering the shape of the particle by including a shape factor that takes a different value for spherical or cylindrical particles. The Bruggeman model and Wasp model are also considered some of the most used classical models (see Ref. [93]). The experimental thermal conductivities of the 1% α-SiC, 2% α-SiC, 1% β-SiC, and 2% β-SiC nanofluids show average deviations of 0.5%, 2.0%, 5.5%, and 9.2%, respectively, with respect to the values predicted by Maxwell's model and Hamilton-Crosser's model for spherical particles, using a k_{np} value of 350 $W \cdot m^{-1} \cdot K^{-1}$ [89]. Thus, the values predicted by these models show good agreement with the experimental thermal conductivities of α-SiC nanofluids but underestimate the experimental values of β-SiC nanofluids, even using a higher k_{np} value of 500 $W\ m^{-1}\ K^{-1}$ [91]. Maxwell's and Hamilton-Crosser's models do not consider the effects of the particle aggregation, interfacial layer or Brownian motion [96,97]. From the previous results it could be affirmed that the thermal conductivity of α-SiC nanofluids behaves similarly to that of classical solid-liquid mixtures, while a greater presence of nanoparticle interaction can be inferred affecting this property in β-SiC nanofluids. Once there are more experimental works on nanofluids with nanoparticles of the same material and different crystal structures, the proposal of models like those from [98,99] but including the crystal structure among the variables to obtain k_{nf} could be the subject of future research.

3.4. Rheological behaviour

Fig. 5a shows the flow curves for PG:W 30:70 and the nanofluids at various temperatures. As can be seen, the dynamic viscosity does not show dependence on the shear rate in the range of analysed values, so all the samples present a Newtonian behaviour within the studied conditions. Table 5 compiles the reported dynamic viscosities of the samples, obtained as the average value in the shear rate range from 100 to 1000 s^{-1}. The η values presented for PG:W 30:70 are consistent with the literature, with average deviations of −1.4%, −6.0%, 0.3%, −2.5%, −0.3%, and − 5.3% with respect to Kapadi et al. [74], Yang et al. [75], Melinder [76], Vallejo et al. [77], Vallejo et al. [100], and Vallejo et al. [101], respectively. Fig. 5b shows the viscosity of the designed samples as a function of temperature. As expected, this property is highly temperature-dependent since a 20 K increase (from 293.15 to 313.15 K) causes the viscosity to be reduced by 47–48% for all samples. It should be noted that there are no differences in this behaviour between the base fluid and nanofluids. The increase in temperature produces a reduction of the cohesion forces between the molecules of the fluids, which causes a decrease in the shear stress, and consequently in the viscosity.

Higher concentrations of SiC nanoparticles in the base fluid lead to increases in the dynamic viscosity, which are greater for β-SiC nanofluids (up to 16–17%) than for α-SiC nanofluids (up to 6–7%). It should be noted that these rises are practically independent of temperature. It can be concluded that SiC with a mostly cubic crystal structure causes

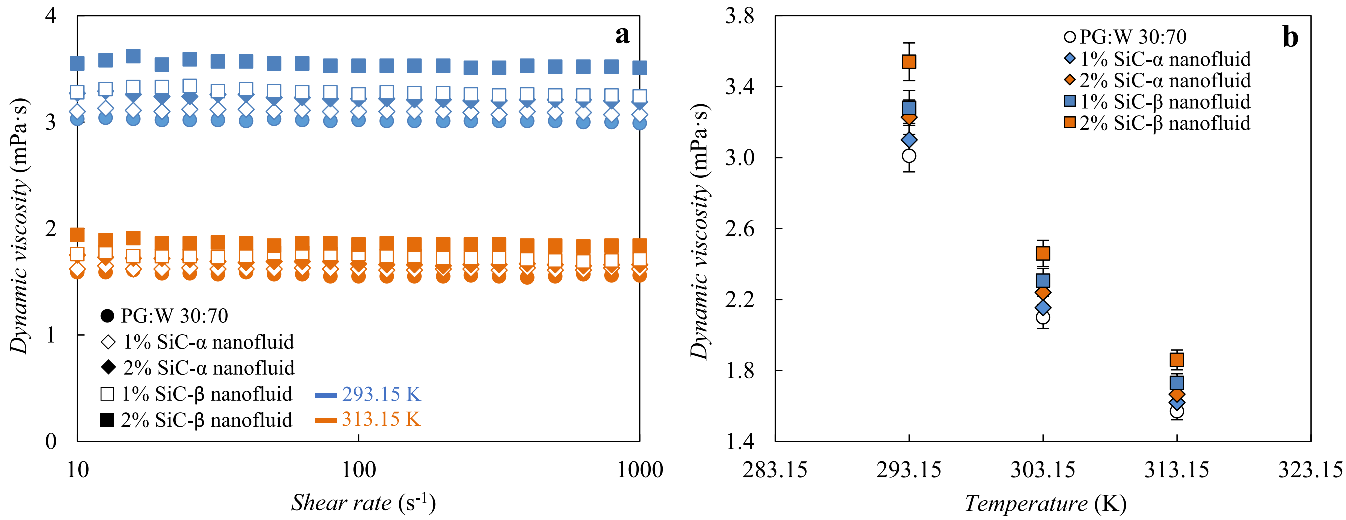

Fig. 5. Flow curves at 293.15 and 313.15 K (a) and average dynamic viscosity values in the shear rate range from 10 to 1000 s^{-1} as a function of temperature (b) for PG:W 30:70 base fluid and α-SiC and β-SiC nanofluids at different concentrations. Error bars inform about the expanded uncertainty (k = 2).

Table 5
Experimental dynamic viscosity values[a] for PG:W 30:70 base fluid and α-SiC and β-SiC nanofluids at different temperatures[b].

Temperature (K)	*Dynamic viscosity* (mPa·s)				
	PG:W 30:70	1% α-SiC nanofluid	2% α-SiC nanofluid	1% β-SiC nanofluid	2% β-SiC nanofluid
293.15	3.01	3.10	3.23	3.28	3.54
303.15	2.10	2.15	2.24	2.31	2.46
313.15	1.57	1.62	1.67	1.73	1.86

[a] Expanded uncertainty of dynamic viscosity (k = 2): 3%.
[b] Expanded uncertainty of temperature (k = 2): 0.1 K.

higher η increments than SiC with a mostly hexagonal crystal structure for a similar size and shape of the nanoparticles. Nikkam et al. [30] obtained similar results for 9 wt% nanofluids based on EG:W 50:50 wt%. They reported a superior increase for β-SiC nanofluids (around 36%) than for α-SiC nanofluids (around 14%). In their case, the larger size of their β-SiC nanoparticles (85–115 nm for α-Si versus 30–60 nm for β-SiC) also contributes to the larger increase.

Several theoretical and empirical models have been proposed for the dynamic viscosity estimation of nanofluids [102]. One of the first theoretical models used with nanofluids was Einstein's model [103], applicable to dispersions of hard spheres without charge in volume concentrations <2%:

$$\eta_{nf} = (1 + 2.5 \cdot \phi_v) \cdot \eta_{bf} \tag{12}$$

where η is dynamic viscosity, ϕ_v is the volume fraction of nanoadditive, and nf and bf mean nanofluid and base fluid, respectively. Brinkman [104] extended the model for concentrations up to 4 vol%, Batchelor [105] included the effect of Brownian motion and particle interaction, or Thomas and Muthukumar [106] considered the three-body hydrodynamic contributions (see the equations corresponding to these models in Ref. [102]). The experimental viscosities of the 1% α-SiC, 2% α-SiC, 1% β-SiC, and 2% β-SiC nanofluids show very similar average deviations of 2.0%, 5.1%, 8.8% and 16%, respectively, with respect to the values predicted by the four theoretical models cited [103–106].

Regarding empirical models, many equations have been proposed in the literature by fitting experimental data [102]. Some of the best known are that of Maïga et al. for Al_2O_3/water nanofluids [107]:

$$\eta_{nf} = \left(1 + 7.23 \cdot \phi_v + 123 \cdot {\phi_v}^2\right) \cdot \eta_{bf} \tag{13}$$

or Chen et al. for TiO_2/EG nanofluids [108]:

$$\eta_{nf} = \left(1 + 10.6 \cdot \phi_v + 10.6 \cdot {\phi_v}^2\right) \cdot \eta_{bf} \tag{14}$$

The experimental viscosities of the 1% α-SiC, 2% α-SiC, 1% β-SiC, and 2% β-SiC nanofluids show absolute average deviations of 0.4%, 1.5%, 7.1%, and 12% from Eq. 13, respectively, and of 0.5%, 0.4%, 6.1% and 10% from Eq. 14, respectively. Thus, the predicted data is in better agreement with the experimental values obtained for the α-SiC nanofluids. However, it is observed that even for the same type of material and base fluid, the correlations are not designed to predict the differences due to the crystal structure of the particles. The proposal of models like those from [109] but including the crystal structure among the variables to obtain η_{nf} could be a subject for future research.

3.5. Isobaric heat capacity

Table 6 gathers the experimental isobaric heat capacities for PG:W 30:70 and the nanofluids at the analysed temperatures. The experimental values we obtained for the base fluid are in accordance with the literature, with absolute average deviations of 3.2% from Yang et al. [110], 0.8% from Melinder [76] and 0.1% from Vallejo et al. [77]. Fig. 6 shows a similar c_p trend with temperature for the base fluid and nanofluids, since all samples present a c_p increase of 1.2–1.3% for the temperature growth from 293.15 to 313.15 K.

As regards to the isobaric heat capacity variation caused by the dispersion of SiC nanoparticles, decreases of up to 2% were detected with increased concentration. The differences between equally concentrated α-SiC and β-SiC nanofluids are within the experimental uncertainty of the measurements, but the c_p values of the β-SiC nanofluids are systematically superior to those of the α-SiC nanofluids, as can be seen in Fig. 6. This is consistent with the small differences between

Table 6
Experimental isobaric heat capacity values[a] for PG:W 30:70 base fluid and α-SiC and β-SiC nanofluids at different temperatures[b].

Temperature (K)	*Isobaric heat capacity* ($J \cdot kg^{-1} \cdot K^{-1}$)				
	PG:W 30:70	1% α-SiC nanofluid	2% α-SiC nanofluid	1% β-SiC nanofluid	2% β-SiC nanofluid
293.15	3830	3787	3753	3798	3768
303.15	3855	3813	3779	3827	3792
313.15	3875	3835	3802	3848	3814

[a] Expanded uncertainty of isobaric heat capacity (k = 2): 3%.
[b] Expanded uncertainty of temperature (k = 2): 0.1 K.

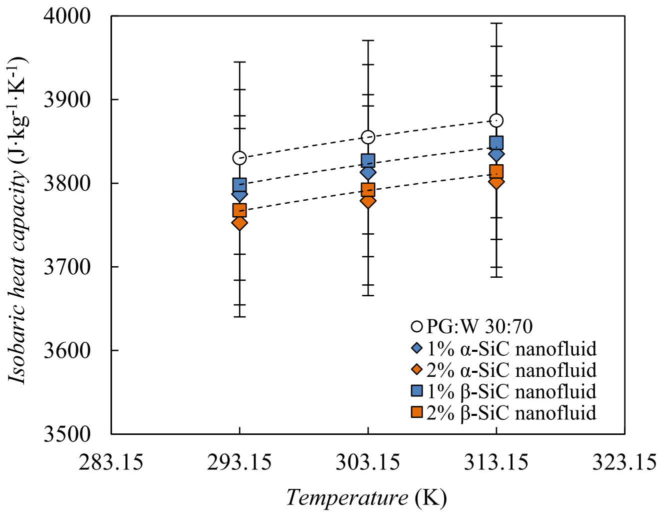

Fig. 6. Isobaric heat capacity as a function of temperature for PG:W 30:70 base fluid and α-SiC and β-SiC nanofluids at different concentrations. The error bars inform about the expanded uncertainty (k = 2). Reference lines are obtained from Xuan and Roetzel's model with $c_{p\ np} = 670$ J·kg^{-1}·K^{-1}, Eq. 16 (−−).

the literature values for the solid phase heat capacities of the different SiC crystal structures. Chase [111] reported c_p values of 672 and 674 J·kg^{-1}·K^{-1} for α-SiC (6H) and β-SiC crystals at 300 K, respectively. Lide [112] reported c_p values of 666 and 671 J·kg^{-1}·K^{-1} for hexagonal and cubic silicon carbide crystals, respectively. The heat capacity of the α phase is slightly lower than that of the β phase in all cases, which could explain its higher contribution to the reduction of the c_p of the corresponding nanofluids.

The thermal equilibrium model for mixtures of materials has been proposed by Xuan and Roetzel [113] and then extensively validated [80,114] to predict the effective isobaric heat capacity of nanofluids:

$$(\rho \cdot c_p)_{nf} = \phi_v \cdot (\rho \cdot c_p)_{np} + (1 - \phi_v) \cdot (\rho \cdot c_p)_{bf} \tag{15}$$

where ρ is density, c_p is isobaric heat capacity, ϕ_v is the volume fraction of nanoadditive, and nf, np and bf mean nanofluid, nanoparticle, and base fluid, respectively. This model provides better accuracy in the c_p prediction than the ideal gases mixing model [115]. Eq. 15 can be simplified by using the nanoparticle mass fraction (ϕ_m) according to the following expression [116]:

$$c_{p\ nf} = \phi_m \cdot c_{p\ np} + (1 - \phi_m) \cdot \rho c_{p\ bf} \tag{16}$$

Using a $c_{p\ np}$ value of 670 J·kg^{-1}·K^{-1}, average deviations of −0.3%, and 0.1% were obtained for the 2% α-SiC and β-SiC nanofluids, respectively. Thus, a good agreement among experimental and predicted data was obtained. There are no significant differences in the $c_{p\ nf}$ prediction using $c_{p\ np}$ values within the aforementioned range of 666 to 674 J·kg^{-1}·K^{-1} [111,117].

3.6. Figures-of-merit

Table 7 shows the convective heat transfer ratios for each of the designed nanofluids, calculated according to Eqs. (2)–(7). As mentioned above, applying the corresponding authors' criteria for the mentioned working conditions, $Mo_{nf}/Mo_{bf} > 1$ and $C_\eta/C_k < 4$ indicate better performance for the nanofluid than for the base fluid.

Regarding the results for laminar flow, it is concluded that all nanofluids improve the heat transfer performance of the base fluid according to both Mo_{nf}/Mo_{bf} and C_η/C_k criteria. The Mo_{nf}/Mo_{bf} ratio, directly related to the improvement in thermal conductivity, shows the best results for the 2% β-SiC nanofluid (1.114 on average). On the other hand, the C_η/C_k ratio, which considers the variations in thermal conductivity and dynamic viscosity, shows the best results for the 1% β-SiC nanofluid (1.502 on average).

Regarding the results for turbulent flow, all Mo_{nf}/Mo_{bf} ratios are very close to or >1. However, the results obtained by using the Dittus-Boelter or Simons expressions, Eqs. (4)–(6), are lower than those obtained by using the Vajjha and Dass expression, Eq. (7). In the first case, all values are practically 1, while in the second case, values of up to 1.4 are achieved. The literature frequently shows values of about 1 [51,59,63] or even clearly lower than 1 [52,61,62] for Eqs. (4)–(6) and higher than 1 [45,66,68,69] for Eq. (7). It can also be concluded that 1% and 2% nanofluids show very similar performances in all cases. The appearance of an optimal nanoparticle concentration for the convective heat transfer performance is a common phenomenon in the nanofluid literature [118]. It is usually related to achieving the best balance between the benefits of enhancing thermal conductivity and the trouble with increasing viscosity.

It should be noted that in both laminar and turbulent flow, see Fig. 7a, all convective heat transfer ratios show better performance when nanoparticles with the least complex crystal structure (β-SiC,

Table 7
Convective heat transfer ratios for laminar and turbulent flow at various temperatures, obtained from Eqs. (2)–(7).

	Temperature (K)	1% α-SiC nanofluid	2% α-SiC nanofluid	1% β-SiC nanofluid	2% β-SiC nanofluid
$\left(\frac{Mo_{nf}}{Mo_{bf}}\right)_{\text{laminar flow}}$	293.15	1.016	1.043	1.065	1.113
	303.15	1.015	1.038	1.062	1.117
	313.15	1.013	1.039	1.067	1.111
$\left(\frac{C_\eta}{C_k}\right)_{\text{laminar flow}}$	293.15	1.897	1.708	1.373	1.564
	303.15	1.541	1.776	1.618	1.465
	313.15	2.447	1.631	1.516	1.670
$\left(\frac{Mo_{nf}}{Mo_{bf}}\right)_{\text{turbulent flow Dittus-Boelter heating}}$	293.15	0.998	1.001	1.006	1.006
	303.15	1.000	1.001	1.000	1.009
	313.15	0.996	1.003	1.003	1.001
$\left(\frac{Mo_{nf}}{Mo_{bf}}\right)_{\text{turbulent flow Dittus-Boelter cooling}}$	293.15	0.998	1.001	1.004	1.002
	303.15	1.001	1.000	0.997	1.006
	313.15	0.995	1.002	1.000	0.996
$\left(\frac{Mo_{nf}}{Mo_{bf}}\right)_{\text{turbulent flow Simons}}$	293.15	0.998	1.001	1.005	1.003
	303.15	1.001	1.000	0.998	1.007
	313.15	0.995	1.002	1.001	0.998
$\left(\frac{Mo_{nf}}{Mo_{bf}}\right)_{\text{turbulent flow Vajjha and Das}}$	293.15	1.383	1.388	1.395	1.398
	303.15	1.334	1.336	1.338	1.351
	313.15	1.290	1.298	1.301	1.302

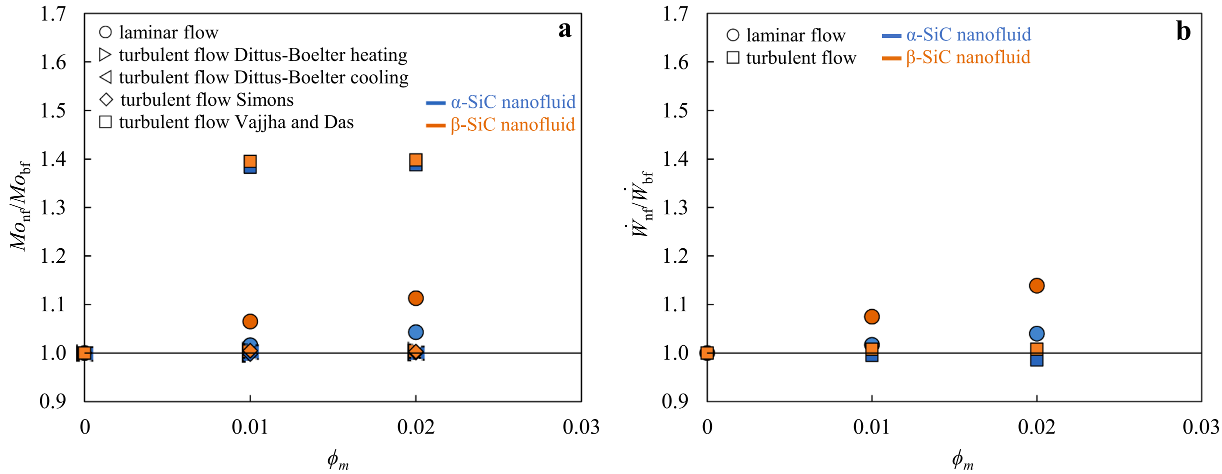

Fig. 7. Mouromtseff number ratio, Mo_{nf}/Mo_{bf}, (a) and pumping power ratio, $\dot{W}_{nf}/\dot{W}_{bf}$, (b) as a function of nanoparticle mass fraction, ϕ_m, at 293.15 K.

cubic) are involved, in line with its greater thermal conductivity and despite its slightly higher viscosity.

Table 8 and Fig. 7b show the pumping power ratios for the designed nanofluids, obtained from Eq. (8) (laminar flow) and Eq. (9) (turbulent flow). As noted in Section 2.2.2., $\dot{W}_{nf}/\dot{W}_{bf} > 1$ indicates that the nanofluid needs more pumping power to flow than the base fluid. The results for laminar flow show small increases of the pumping power requirements for nanofluids. These requirements are higher for β-SiC than for α-SiC nanofluids and increase with concentration, reaching ~14% for the 2% β-SiC nanofluid. The results for turbulent flow show pumping power ratios of about 1, which means that the pumping power requirements are practically identical to those of the base fluid for this flow regime.

The experimental study of the heat transfer and pressure drop of the proposed nanofluids in real installations over tube or plate heat exchangers (as in [119,120]) and the proposal of models that include the crystal structure among the variables to obtain *h* or *Nu* (as in [121,122]) could be an aim for future research.

4. Conclusions

The study of the stability, thermophysical profile and figures-of-merit of SiC nanofluids with different crystal structures revealed a great potential for use in convection applications. The main conclusions are summarised below:

1) New nanofluids based on the PG:W 30:70 mixture were designed, consisting of dispersions at 1 and 2 wt% concentrations of α-SiC and β-SiC nanopowders with a majority presence of the 6H and 3C polytypes, respectively. Zeta potential evaluations of the nanofluids demonstrate moderately stable dispersions.
2) The SiC crystal structure does not show a noticeable influence in density and isobaric heat capacity of the nanofluids. The Pak and Cho and Xuan and Roetzel models show good predictions of the respective experimental data.
3) The SiC crystal structure plays a noticeable role in the thermal conductivity enhancement of the nanofluids. Temperature-independent rises of up to 4% and 11–12% were obtained for the 2% α-SiC and β-SiC nanofluids, respectively. Thus, the nanomaterial with the least complex crystal structure (β-SiC, cubic) improves the thermal conductivity of the fluid in which it is dispersed more than those with the most complex crystal structure (α-SiC, hexagonal).
4) The flow curves of the base fluid and all nanofluids show the Newtonian behaviour of the samples. The SiC crystal structure affects the dynamic viscosity increase of the nanofluids. Temperature-independent increases of up to 6–7% and 16–17% were obtained for 2% α-SiC and β-SiC nanofluids, respectively.
5) The Mo_{nf}/Mo_{bf} and C_η/C_k ratios for laminar flow indicate a higher convection heat transfer performance for the nanofluids than for the base fluid. On the other hand, the Mo_{nf}/Mo_{bf} ratios for turbulent flow indicate similar or greater performances.
6) Based on figures-of-merit, the nanofluids containing the nanoparticles with the least complex crystal structure (β-SiC, cubic) demonstrate better prospects for use in convection applications in exchange for a small pumping power increase.
7) The experimental study of the performance of the proposed nanofluids in tube or plate heat exchangers may be the subject for future research. Likewise, the proposal of models that include the crystal structure among the variables to obtain *k*, *η*, *h*, or *Nu* (among others) could also be considered.

CRediT authorship contribution statement

Javier P. Vallejo: Conceptualization, Data curation, Formal analysis, Investigation, Methodology, Writing – original draft, Writing – review & editing, Funding acquisition. **Lara Febrero-Garrido:** Data curation, Formal analysis, Investigation, Methodology, Writing – review & editing. **Antón Cacabelos:** Formal analysis, Investigation, Writing – review & editing. **Arturo González-Gil:** Formal analysis, Investigation, Writing – review & editing. **Luis Lugo:** Formal analysis, Funding acquisition, Investigation, Writing – review & editing.

Table 8
Pumping power ratios at various temperatures, obtained from Eq. (8)–(9).

	Temperature (K)	1% α-SiC nanofluid	2% α-SiC nanofluid	1% β-SiC nanofluid	2% β-SiC nanofluid
$\left(\frac{\dot{W}_{nf}}{\dot{W}_{bf}}\right)_{laminar\ flow}$	293.15	1.017	1.040	1.075	1.139
	303.15	1.011	1.034	1.086	1.135
	313.15	1.019	1.033	1.087	1.149
$\left(\frac{\dot{W}_{nf}}{\dot{W}_{bf}}\right)_{turbulent\ flow}$	293.15	0.995	0.986	1.008	1.008
	303.15	0.994	0.985	1.011	1.008
	313.15	0.995	0.986	1.011	1.012

Declaration of Competing Interest

The authors declare no conflict of interest.

Data availability

Data will be made available on request.

Acknowledgements

The authors thank the Defense University Center at the Spanish Naval Academy (CUD-ENM) for the support provided for this research through the project PICUD2022-07. Grant PID2020-112846RB-C21 funded by MCIN/AEI/10.13039/501100011033. Grant PDC2021-121225-C21 funded by MCIN/AEI/10.13039/501100011033 and by "European Union NextGenerationEU/PRTR".

References

[1] European Commission, Energy Performance of Buildings Directive. https://energy.ec.europa.eu/topics/energy-efficiency/energy-efficient-buildings/energy-performance-buildings-directive_en, 2018.

[2] F.E. Abrahamsen, S.G. Ruud, A. Gebremedhin, Assessing efficiency and environmental performance of a nearly zero-energy university building's energy system in Norway, Buildings. 13 (2023) 169.

[3] S. Qu, J. Han, Z. Sun, R. Yin, R. Ji, C. Chai, Study of operational strategies for a hybrid solar-geothermal heat pump system, in: Build. Simul., Springer, 2019, pp. 697–710.

[4] M.A. Perea-Moreno, F. Manzano-Agugliaro, A.J. Perea-Moreno, Sustainable energy based on sunflower seed husk boiler for residential buildings, Sustainability. 10 (2018) 3407.

[5] P. Cui, W. Yang, W. Zhang, K. Zhu, J.D. Spitler, M. Yu, Advances in ground heat exchangers for space heating and cooling: review and perspectives, energy, Built Environ. 5 (2024) 255–269.

[6] J.P. Vallejo, J.I. Prado, L. Lugo, Hybrid or mono nanofluids for convective heat transfer applications. A critical review of experimental research, Appl. Therm. Eng. 203 (2022), 117926.

[7] B. Mehta, D. Subhedar, H. Panchal, Z. Said, Synthesis, stability, thermophysical properties and heat transfer applications of nanofluid–a review, J. Mol. Liq. 120034 (2022).

[8] A.R.I. Ali, B. Salam, A review on nanofluid: preparation, stability, thermophysical properties, heat transfer characteristics and application, SN Appl. Sci. 2 (2020) 1636.

[9] A.G.N. Sofiah, M. Samykano, A.K. Pandey, K. Kadirgama, K. Sharma, R. Saidur, Immense impact from small particles: review on stability and thermophysical properties of nanofluids, Sustain. Energy Technol. Assess. 48 (2021), 101635.

[10] G. Yıldız, Ü. Ağbulut, A.E. Gürel, A review of stability, thermophysical properties and impact of using nanofluids on the performance of refrigeration systems, Int. J. Refrig. 129 (2021) 342–364.

[11] M.C. Wingert, J. Zheng, S. Kwon, R. Chen, Thermal transport in amorphous materials: a review, Semicond. Sci. Technol. 31 (2016), 113003.

[12] W. Zhou, Y. Cheng, K. Chen, G. Xie, T. Wang, G. Zhang, Thermal conductivity of amorphous materials, Adv. Funct. Mater. 30 (2020) 1903829.

[13] X. Zhang, L.-D. Zhao, Thermoelectric materials: energy conversion between heat and electricity, J. Mater. 1 (2015) 92–105.

[14] P.F. Lory, V.M. Giordano, P. Gille, H. Euchner, M. Mihalkovič, E. Pellegrini, M. Gonzalez, L.-P. Regnault, P. Bastie, H. Schober, Impact of structural complexity and disorder on lattice dynamics and thermal conductivity in the o-$Al_{13}Co_4$ phase, Phys. Rev. B 102 (2020), 024303.

[15] H. Abderrazak, E. Hmida, Silicon carbide: synthesis and properties, in: Properties and Applications of Silicon Carbide, InTech Rijeka, 2011, pp. 361–388.

[16] P.M. Sarro, Silicon carbide as a new MEMS technology, Sens. Actuators A Phys. 82 (2000) 210–218.

[17] H. Jian-Feng, Z. Xie-Rong, L. He-Jun, X. Xin-Bo, F. Ye-Wei, Influence of the preparation temperature on the phase, microstructure and anti-oxidation property of a SiC coating for C/C composites, Carbon. 42 (2004) 1517–1521.

[18] V. Parshin, E. Serov, G. Denisov, B. Garin, R. Denisyuk, V. V'yuginov, V. Klevtsov, N. Travin, Silicon carbide for high-power applications at MM and THz ranges, Diam. Relat. Mater. 80 (2017) 1–4.

[19] D. Singh, E.V. Timofeeva, W. Yu, J. Routbort, D. France, D. Smith, J.M. Lopez-Cepero, An investigation of silicon carbide-water nanofluid for heat transfer applications, J. Appl. Phys. 105 (2009), 064306.

[20] W. Yu, D.M. France, D.S. Smith, D. Singh, E.V. Timofeeva, J.L. Routbort, Heat transfer to a silicon carbide/water nanofluid, Int. J. Heat Mass Transf. 52 (2009) 3606–3612.

[21] X. Li, C. Zou, X. Lei, W. Li, Stability and enhanced thermal conductivity of ethylene glycol-based SiC nanofluids, Int. J. Heat Mass Transf. 89 (2015) 613–619.

[22] X. Li, C. Zou, T. Wang, X. Lei, Rheological behavior of ethylene glycol-based SiC nanofluids, Int. J. Heat Mass Transf. 84 (2015) 925–930.

[23] X. Li, C. Zou, Thermo-physical properties of water and ethylene glycol mixture based SiC nanofluids: an experimental investigation, Int. J. Heat Mass Transf. 101 (2016) 412–417.

[24] X. Li, C. Zou, A. Qi, Experimental study on the thermo-physical properties of car engine coolant (water/ethylene glycol mixture type) based SiC nanofluids, Int. Commun. Heat Mass Transf. 77 (2016) 159–164.

[25] X. Li, C. Zou, L. Zhou, A. Qi, Experimental study on the thermo-physical properties of diathermic oil based SiC nanofluids for high temperature applications, Int. J. Heat Mass Transf. 97 (2016) 631–637.

[26] E.V. Timofeeva, D.S. Smith, W. Yu, D.M. France, D. Singh, J.L. Routbort, Particle size and interfacial effects on thermo-physical and heat transfer characteristics of water-based α-SiC nanofluids, Nanotechnology. 21 (2010), 215703.

[27] E.V. Timofeeva, W. Yu, D.M. France, D. Singh, J.L. Routbort, Base fluid and temperature effects on the heat transfer characteristics of SiC in ethylene glycol/H_2O and H_2O nanofluids, J. Appl. Phys. 109 (2011), 014914.

[28] S. Hosseini, A. Moghadassi, D. Henneke, A. Elkamel, The thermal conductivities enhancement of mono ethylene glycol and paraffin fluids by adding β-SiC nanoparticles, J. Therm. Anal. Calorim. 101 (2010) 113–118.

[29] A.H.A. Al-Waeli, K. Sopian, M.T. Chaichan, H.A. Kazem, H.A. Hasan, A.N. Al-Shamani, An experimental investigation of SiC nanofluid as a base-fluid for a photovoltaic thermal PV/T system, Energy Convers. Manag. 142 (2017) 547–558.

[30] G. Huminic, A. Huminic, C. Fleaca, F. Dumitrache, I. Morjan, Thermo-physical properties of water based SiC nanofluids for heat transfer applications, Int. Commun. Heat Mass Transfr. 84 (2017) 94–101.

[31] S. Akilu, A.T. Baheta, K. Kadirgama, E. Padmanabhan, K.V. Sharma, Viscosity, electrical and thermal conductivities of ethylene and propylene glycol-based β-SiC nanofluids, J. Mol. Liq. 284 (2019) 780–792.

[32] H. Xie, J. Wang, T. Xi, Y. Liu, Thermal conductivity of suspensions containing nanosized SiC particles, Int. J. Thermophys. 23 (2002) 571–580.

[33] S.W. Lee, S.D. Park, S. Kang, I.C. Bang, J.H. Kim, Investigation of viscosity and thermal conductivity of SiC nanofluids for heat transfer applications, Int. J. Heat Mass Transf. 54 (2011) 433–438.

[34] O. Manna, S.K. Singh, G. Paul, Enhanced thermal conductivity of nano-SiC dispersed water based nanofluid, Bull. Mater. Sci. 35 (2012) 707–712.

[35] N. Nikkam, E.B. Haghighi, M. Saleemi, M. Behi, R. Khodabandeh, M. Muhammed, B. Palm, M.S. Toprak, Experimental study on preparation and base liquid effect on thermo-physical and heat transport characteristics of α-SiC nanofluids, Int. Commun. Heat Mass Transf. 55 (2014) 38–44.

[36] N. Nikkam, M. Saleemi, E.B. Haghighi, M. Ghanbarpour, R. Khodabandeh, M. Muhammed, B. Palm, M.S. Toprak, Fabrication, characterization and thermophysical property evaluation of SiC nanofluids for heat transfer applications, Nano Lett. 6 (2014) 178–189.

[37] S. Akilu, K.V. Sharma, T.B. Aklilu, M.S.M. Azman, P.T. Bhaskoro, Temperature dependent properties of silicon carbide nanofluid in binary mixtures of glycerol-ethylene glycol, Procedia Eng. 148 (2016) 774–778.

[38] W. Yu, M. Wang, H. Xie, Y. Hu, L. Chen, Silicon carbide nanowires suspensions with high thermal transport properties, Appl. Therm. Eng. 94 (2016) 350–354.

[39] W. Chen, C. Zou, X. Li, L. Li, Experimental investigation of SiC nanofluids for solar distillation system: stability, optical properties and thermal conductivity with saline water-based fluid, Int. J. Heat Mass Transf. 107 (2017) 264–270.

[40] W. Chen, C. Zou, X. Li, An investigation into the thermophysical and optical properties of SiC/ionic liquid nanofluid for direct absorption solar collector, Sol. Energy Mater. Sol. Cells 163 (2017) 157–163.

[41] C. Ezekwem, A. Dare, Thermal and electrical conductivity of silicon carbide nanofluids, Energ. Source Part A. (2020) 1–19.

[42] G.L. Harris (Ed.), Properties of Silicon Carbide, INSPEC, 1995.

[43] A.H. de Gomes, de Mesquita, Refinement of the crystal structure of SiC type 6H, Acta Crystallogr. 23 (1967) 610–617.

[44] G. Żyła, J.P. Vallejo, J. Fal, L. Lugo, Nanodiamonds – ethylene glycol nanofluids: experimental investigation of fundamental physical properties, Int. J. Heat Mass Transf. 121 (2018) 1201–1213.

[45] J.P. Vallejo, E. Álvarez-Regueiro, D. Cabaleiro, J. Fernández-Seara, J. Fernández, L. Lugo, Functionalized graphene nanoplatelet nanofluids based on a commercial industrial antifreeze for the thermal performance enhancement of wind turbines, Appl. Therm. Eng. 152 (2019) 113–125.

[46] D. Cabaleiro, C. Gracia-Fernández, L. Lugo, (solid+ liquid) phase equilibria and heat capacity of (diphenyl ether+ biphenyl) mixtures used as thermal energy storage materials, J. Chem. Thermodyn. 74 (2014) 43–50.

[47] K.S. Suganthi, K.S. Rajan, Metal oxide nanofluids: Review of formulation, thermo-physical properties, mechanisms, and heat transfer performance, Renew. Sust. Energ. Rev. 76 (2017) 226–255.

[48] E.B. Elcioglu, A.M. Genc, Z.H. Karadeniz, M.A. Ezan, A. Turgut, Nanofluid figure-of-merits to assess thermal efficiency of a flat plate solar collector, Energy Convers. Manag. 204 (2020), 112292.

[49] W. Yu, D.M. France, E.V. Timofeeva, D. Singh, J.L. Routbort, Comparative review of turbulent heat transfer of nanofluids, Int. J. Heat Mass Transf. 55 (2012) 5380–5396.

[50] R.E. Simons, Comparing heat transfer rates of liquid coolants using the Mouromtseff number, Electronic Cooling. 12 (2006).

[51] A.A. Minea, M.G. Moldoveanu, Studies on Al_2O_3, CuO, and TiO_2 water-based nanofluids: a comparative approach in laminar and turbulent flow, J. Eng. Thermophys. 26 (2017) 291–301.

[52] G. Żyła, J. Fal, Viscosity, thermal and electrical conductivity of silicon dioxide–ethylene glycol transparent nanofluids: an experimental studies, Thermochim. Acta 650 (2017) 106–113.

[53] M. Leena, S. Srinivasan, Experimental investigation of the thermophysical properties of TiO 2/propylene glycol–water nanofluids for heat-transfer applications, J. Eng. Phys. Thermophys. 91 (2018) 498–506.
[54] Y. Zhai, L. Li, J. Wang, Z. Li, Evaluation of surfactant on stability and thermal performance of Al2O3-ethylene glycol (EG) nanofluids, Powder Technol. 343 (2019) 215–224.
[55] R. Gómez-Villarejo, P. Estellé, J. Navas, Boron nitride nanotubes-based nanofluids with enhanced thermal properties for use as heat transfer fluids in solar thermal applications, Sol. Energy Mater. Sol. Cells 205 (2020), 110266.
[56] R. Prasher, D. Song, J. Wang, P. Phelan, Measurements of nanofluid viscosity and its implications for thermal applications, Appl. Phys. Lett. 89 (2006).
[57] W. Yu, D.M. France, D.S. Smith, D. Singh, E.V. Timofeeva, J.L. Routbort, Heat transfer to a silicon carbide/water nanofluid, Int. J. Heat Mass Transf. 52 (2009) 3606–3612.
[58] R. Mondragón, C. Segarra, J.C. Jarque, J.E. Julia, L. Hernández, R. Martínez-Cuenca, Characterization of physical properties of nanofluids for heat transfer application, in: J. Phys. Conf. Ser., IOP Publishing, 2012, p. 012017.
[59] W. Yu, E.V. Timofeeva, D. Singh, D.M. France, R.K. Smith, Investigations of heat transfer of copper-in-Therminol 59 nanofluids, Int. J. Heat Mass Transf. 64 (2013) 1196–1204.
[60] P. Dehury, U. Mahanta, T. Banerjee, Comprehensive assessment on the use of boron nitride-based nanofluids comprising eutectic mixtures of diphenyl ether and menthol for enhanced thermal media, ACS Sustain. Chem. Eng. 8 (2020) 14595–14604.
[61] L.S. Sundar, M.J. Hortiguela, M.K. Singh, A.C.M. Sousa, Thermal conductivity and viscosity of water based nanodiamond (ND) nanofluids: an experimental study, Int. Commun. Heat Mass Transf. 76 (2016) 245–255.
[62] G. Huminic, A. Huminic, Heat transfer capability of the hybrid nanofluids for heat transfer applications, J. Mol. Liq. 272 (2018) 857–870.
[63] H. Zhang, S. Qing, Y. Zhai, X. Zhang, A. Zhang, The changes induced by pH in TiO2/water nanofluids: stability, thermophysical properties and thermal performance, Powder Technol. 377 (2021) 748–759.
[64] P.M. Kumar, R. Parameshwaran, I. Sreedhar, Thermal conductivity enhancement of magnetic nanofluids for energy applications, Mater. Today Proc. 72 (2023) 67–73.
[65] R.S. Vajjha, D.K. Das, A review and analysis on influence of temperature and concentration of nanofluids on thermophysical properties, heat transfer and pumping power, Int. J. Heat Mass Transf. 55 (2012) 4063–4078.
[66] D. Cabaleiro, L. Colla, F. Agresti, L. Lugo, L. Fedele, Transport properties and heat transfer coefficients of ZnO/(ethylene glycol+ water) nanofluids, Int. J. Heat Mass Transf. 89 (2015) 433–443.
[67] M.M. Ehsan, S. Noor, S. Salehin, A.K.M.S. Islam, Application of nanofluid in heat exchangers for energy savings, in: Thermofluid Modeling for Energy Efficiency Applications, Elsevier, 2016, pp. 73–101.
[68] G. Huminic, A. Vărdaru, A. Huminic, C. Fleacă, F. Dumitrache, I. Morjan, Water-based graphene oxide–silicon hybrid nanofluids—experimental and theoretical approach, Int. J. Mol. Sci. 23 (2022) 3056.
[69] A. Dosodia, S. Vadapalli, A.K. Jain, S.B. Mukkamala, B.T. Sanduru, Experimental studies and analytical analysis of thermophysical properties of ethylene glycol–water-based nanofluids dispersed with multi-walled carbon nanotubes, Int. J. Thermophys. 43 (2022) 175.
[70] R. Ben Mansour, N. Galanis, C.T. Nguyen, Effect of uncertainties in physical properties on forced convection heat transfer with nanofluids, Appl. Therm. Eng. 27 (2007) 240–249.
[71] A. Ghadimi, R. Saidur, H.S.C. Metselaar, A review of nanofluid stability properties and characterization in stationary conditions, Int. J. Heat Mass Transf. 54 (2011) 4051–4068.
[72] S.K. Babita, S.M. Sharma, Gupta, Preparation and evaluation of stable nanofluids for heat transfer application: a review, Exp. Thermal Fluid Sci. 79 (2016) 202–212.
[73] J.R. Verlinde, R.M.H. Verbeeck, H.P. Thun, Density and vapour pressure of the propylene glycol-water system from 15 to 50°C, Bull. Soc. Chim. Belg. 84 (1975) 1119–1130.
[74] U.R. Kapadi, D.G. Hundiwale, N.B. Patil, M.K. Lande, P.R. Patil, Studies of viscosity and excess molar volume of binary mixtures of propane-1, 2 diol with water at various temperatures, Fluid Phase Equilib. 192 (2001) 63–70.
[75] C.S. Yang, P.S. Ma, D.Q. Tang, F.M. Jin, Excess molar volume, viscosity and heat capacity for the mixture of 1,2-propanediol-water at different temperatures, Chin. J. Chem. Eng. 11 (2003) 175–180.
[76] Å. Melinder, Properties of Secondary Work Fluidsfor Indirect Systems, International Institute of Refrigeration, 2010.
[77] J.P. Vallejo, J. Pérez-Tavernier, D. Cabaleiro, J. Fernández-Seara, L. Lugo, Potential heat transfer enhancement of functionalized graphene nanoplatelet dispersions in a propylene glycol-water mixture. Thermophysical profile, J. Chem. Thermodyn. 123 (2018) 174–184.
[78] B.C. Pak, Y.I. Cho, Hydrodynamic and heat transfer study of dispersed fluids with submicron metallic oxide particles, Experimental Heat Transfer Int. J. 11 (1998) 151–170.
[79] R.S. Vajjha, D.K. Das, B.M. Mahagaonkar, Density measurement of different nanofluids and their comparison with theory, Pet. Sci. Technol. 27 (2009) 612–624.
[80] G. Żyła, J.P. Vallejo, L. Lugo, Isobaric heat capacity and density of ethylene glycol based nanofluids containing various nitride nanoparticle types: an experimental study, J. Mol. Liq. 261 (2018) 530–539.
[81] O.K. Bates, G. Hazzard, Thermal conductivity of alcohols and glycols, Ind. Eng. Chem. 37 (1945) 193–195.
[82] Y. Goldberg, M.E. Levinshtein, S.L. Rumyantsev, Silicon Carbide (SiC), in: M. E. Levinshtein, S.L. Rumyantsev, M.S. Shur (Eds.), Properties of Advanced Semiconductor Materials: GaN, AIN, InN, BN, SiC, SiGe, John Wiley & Sons, New York, 2001, pp. 93–148.
[83] G.A. Slack, Thermal conductivity of pure and impure silicon, silicon carbide, and diamond, J. Appl. Phys. 35 (1964) 3460–3466.
[84] E.A. Burgemeister, W. Von Muench, E. Pettenpaul, Thermal conductivity and electrical properties of 6H silicon carbide, J. Appl. Phys. 50 (1979) 5790–5794.
[85] D.T. Morelli, J.P. Heremans, C.P. Beetz, W.S. Yoo, H. Matsunami, Phonon-electron scattering in single crystal silicon carbide, Appl. Phys. Lett. 63 (1993) 3143–3145.
[86] S.G. Müller, R. Eckstein, D. Hofmann, J. Fricke, R. Horn, H. Mehling, O. Nilsson, R. Hofmann, Experimental and theoretical analysis of the high temperature thermal conductivity of monocrystalline SiC, in: Materials Science Forum, 1998.
[87] X. Qian, P. Jiang, R. Yang, Anisotropic thermal conductivity of 4H and 6H silicon carbide measured using time-domain thermoreflectance, Mater. Today Phys. 3 (2017) 70–75.
[88] Q. Zheng, C. Li, A. Rai, J.H. Leach, D.A. Broido, D.G. Cahill, Thermal conductivity of GaN, GaN 71, and SiC from 150 K to 850 K, Phys. Rev. Mater. 3 (2019), 014601.
[89] Z. Cheng, W. Lu, J. Shi, D. Tanaka, N.H. Protik, S. Wang, M. Iwaya, T. Takeuchi, S. Kamiyama, I. Akasaki, Quasi-ballistic thermal conduction in 6H–SiC, Mater. Today Phys. 20 (2021), 100462.
[90] A. Katre, J. Carrete, B. Dongre, G.K.H. Madsen, N. Mingo, Exceptionally strong phonon scattering by B substitution in cubic SiC, Phys. Rev. Lett. 119 (2017), 075902.
[91] Z. Cheng, J. Liang, K. Kawamura, H. Zhou, H. Asamura, H. Uratani, J. Tiwari, S. Graham, Y. Ohno, Y. Nagai, High thermal conductivity in wafer-scale cubic silicon carbide crystals, Nat. Commun. 13 (2022) 7201.
[92] K.Y. Lim, T.Y. Cho, Y.W. Kim, S.J. Lee, Effect of initial alpha-SiC content on thermal conductivity of silicon carbide ceramics, Key Eng. Mater. 616 (2014) 23–26.
[93] P.M. Kumar, J. Kumar, R. Tamilarasan, S. Sendhilnathan, S. Suresh, Review on nanofluids theoretical thermal conductivity models, Engl. J. 19 (2015) 67–83.
[94] J.C. Maxwell, A Treatise on Electricity and Magnetism, Clarendon Press, 1873.
[95] R.L. Hamilton, O.K. Crosser, Thermal conductivity of heterogeneous two-component systems, Ind. Eng. Chem. Fundam. 1 (1962) 187–191.
[96] I.H. Rizvi, A. Jain, S.K. Ghosh, P.S. Mukherjee, Mathematical modelling of thermal conductivity for nanofluid considering interfacial nano-layer, Heat Mass Transf. 49 (2013) 595–600.
[97] J. Li, X. Zhang, B. Xu, M. Yuan, Nanofluid research and applications: a review, Int. Commun. Heat Mass Transf. 127 (2021), 105543.
[98] F. Soltani, D. Toghraie, A. Karimipour, Experimental measurements of thermal conductivity of engine oil-based hybrid and mono nanofluids with tungsten oxide (WO_3) and MWCNTs inclusions, Powder Technol. 371 (2020) 37–44.
[99] A. Boroomandpour, D. Toghraie, M. Hashemian, A comprehensive experimental investigation of thermal conductivity of a ternary hybrid nanofluid containing MWCNTs-titania-zinc oxide/water-ethylene glycol (80:20) as well as binary and mono nanofluids, Synth. Met. 268 (2020), 116501.
[100] J.P. Vallejo, S. Gómez-Barreiro, D. Cabaleiro, C. Gracia-Fernández, J. Fernández-Seara, L. Lugo, Flow behaviour of suspensions of functionalized graphene nanoplatelets in propylene glycol–water mixtures, Int. Commun. Heat Mass Transf. 91 (2018) 150–157.
[101] J.P. Vallejo, G. Żyła, J. Fernández-Seara, L. Lugo, Rheological behaviour of functionalized graphene nanoplatelet nanofluids based on water and propylene glycol:water mixtures, Int. Commun. Heat Mass Transf. 99 (2018) 43–53.
[102] A. Hemmati-Sarapardeh, A. Varamesh, M.M. Husein, K. Karan, On the evaluation of the viscosity of nanofluid systems: modeling and data assessment, Renew. Sust. Energ. Rev. 81 (2018) 313–329.
[103] A. Einstein, Eine neue Bestimmung der Moleküldimensionen, Ann. Phys. 324 (1906) 289–306.
[104] H.C. Brinkman, The viscosity of concentrated suspensions and solutions, J. Chem. Phys. 20 (1952) 571.
[105] G.K. Batchelor, The effect of Brownian motion on the bulk stress in a suspension of spherical particles, J. Fluid Mech. 83 (1977) 97–117.
[106] C.U. Thomas, M. Muthukumar, Three-body hydrodynamic effects on viscosity of suspensions of spheres, J. Chem. Phys. 94 (1991) 5180–5189.
[107] S.E.B. Maïga, C.T. Nguyen, N. Galanis, G. Roy, Heat transfer behaviours of nanofluids in a uniformly heated tube, Superlattice. Microst. 35 (2004) 543–557.
[108] H. Chen, Y. Ding, Y. He, C. Tan, Rheological behaviour of ethylene glycol based titania nanofluids, Chem. Phys. Lett. 444 (2007) 333–337.
[109] M.H. Ahmadi, B. Mohseni-Gharyehsafa, M. Ghazvini, M. Goodarzi, R.D. Jilte, R. Kumar, Comparing various machine learning approaches in modeling the dynamic viscosity of CuO/water nanofluid, J. Therm. Anal. Calorim. 139 (2020) 2585–2599.
[110] C.S. Yang, P.S. Ma, D.Q. Tang, F.M. Jin, Excess molar volume, viscosity and heat capacity for the mixture of 1,2-propanediol-water at different temperatures, Chin. J. Chem. Eng. 11 (2003) 175–180.
[111] M.W. Chase, NIST-JANAF Thermochemical Tables, Fourth Edition, J. Phys. Chem. Ref. Data, Monograph 9, 1998.
[112] D.R. Lide, CRC Handbook of Chemistry and Physics, CRC Press, 2004.
[113] Y. Xuan, W. Roetzel, Conceptions for heat transfer correlation of nanofluids, Int. J. Heat Mass Transf. 43 (2000) 3701–3707.
[114] D. Shin, D. Banerjee, Enhancement of specific heat capacity of high-temperature silica-nanofluids synthesized in alkali chloride salt eutectics for solar thermal-energy storage applications, Int. J. Heat Mass Transf. 54 (2011) 1064–1070.

[115] I.M. Shahrul, I.M. Mahbubul, S.S. Khaleduzzaman, R. Saidur, M.F.M. Sabri, A comparative review on the specific heat of nanofluids for energy perspective, Renew. Sust. Energ. Rev. 38 (2014) 88–98.
[116] T.P. Teng, Y.H. Hung, Estimation and experimental study of the density and specific heat for alumina nanofluid, J. Exp. Nanosci. 9 (2014) 707–718.
[117] D.R. Lide, CRC Handbook of Chemistry and Physics, CRC Press, 2004.
[118] J.P. Vallejo, U. Calviño, I. Freire, J. Fernández-Seara, L. Lugo, Convective heat transfer in pipe flow for glycolated water-based carbon nanofluids. A thorough analysis, J. Mol. Liq. 301 (2020), 112370.
[119] J.P. Vallejo, L. Ansia, U. Calviño, M.A. Marcos, J. Fernández-Seara, L. Lugo, Convection behaviour of mono and hybrid nanofluids containing B_4C and TiB_2 nanoparticles, Int. J. Therm. Sci. 189 (2023), 108268.
[120] W. Ajeeb, R.R.S.T. da Silva, S.M.S. Murshed, Experimental investigation of heat transfer performance of Al_2O_3 nanofluids in a compact plate heat exchanger, Appl. Therm. Eng. 218 (2023), 119321.
[121] A. Arabpour, A. Karimipour, D. Toghraie, The study of heat transfer and laminar flow of kerosene/multi-walled carbon nanotubes (MWCNTs) nanofluid in the microchannel heat sink with slip boundary condition, J. Therm. Anal. Calorim. 131 (2018) 1553–1566.
[122] E. Khodabandeh, S.A. Rozati, M. Joshaghani, O.A. Akbari, S. Akbari, D. Toghraie, Thermal performance improvement in water nanofluid/GNP–SDBS in novel design of double-layer microchannel heat sink with sinusoidal cavities and rectangular ribs, J. Therm. Anal. Calorim. 136 (2019) 1333–1345.